J. Phys. A: Math. Gen. **29** (1996) 5157–5179. Printed in the UK

The spatial distribution of the illumination of dynamic apertures and its effect on the decay rate of the radiated localized pulses

Amr M Shaarawi†, Sherif M Sedky†, Richard W Ziolkowski‡ and Ioannis M Besieris§

† Department of Engineering Physics and Mathematics, Faculty of Engineering, Cairo University, Giza, Egypt

‡ Electromagnetics Laboratory, Department of Electrical and Computer Engineering, The University of Arizona, Tuscon, AZ 85721, USA

§ Bradley Department of Electrical Engineering, Virginia Polytechnic Institute and State University, Blacksburg, VA 24061, USA

Received 21 June 1995

Abstract. Various illumination schemes of dynamic apertures are investigated. The decay patterns of the generated ultra-wide bandwidth pulses are studied and compared to postulated diffraction lengths. It is shown that such definitions of the diffraction ranges characterize the propagation of the pulses in a broad sense. We emphasize the fact that to understand how a localized pulse decays we have to resort to the structure of its temporal and spatial spectral content. An exhaustive analysis of the depletion of the spectral components of the radiated localized pulses is presented.

1. Introduction

It has been demonstrated that finite-energy causal localized waves (LW) can be generated from dynamic Gaussian apertures [1–3]. These sources are characterized by apertures that vary with time. Such apertures can launch close approximations to the focus wave mode (FWM) pulse [1]. In contradistinction to the source-free FWM field [4, 5], the corresponding LW generated by a dynamic Gaussian aperture is completely causal [1, 2]. It should be emphasized, however, that a condition which allows forward-going components to dominate the source-free FWM pulse [2] has to be imposed in order to ensure that a localized pulse is efficiently launched out of a dynamic Gaussian aperture.

The field illuminating the dynamic aperture has an ultra-wide frequency bandwidth and exhibits a strong correlation between its spatial and temporal spectral components [1]. A clever design of the connection between these components can affect the range through which the pulse travels before it starts decaying. It can, also, significantly alter the rate of decay of the pulse. In this work, we illustrate this point by studying the propagation characteristics of three distinct localized fields. The first is the usual FWM pulse. The other two LW solutions contain higher frequency components and have larger bandwidths. To have a finite energy source, the illumination of the aperture is turned on at $t = -4T$ and then turned off at $t = +4T$ by utilizing a Gaussian time-window of the form $e^{-t^2/4T^2}$. Such a window allows the radius of the aperture to shrink for all negative times from its largest

0305-4470/96/165157+23$19.50 © 1996 IOP Publishing Ltd

size at $t = -4T$, to acquire its minimum radius at $t = 0$, and expand back for all positive times to reach its original size at $t = +4T$ when the illuminating field is turned off.

In this work, we shall provide a detailed analysis of the spectral contents of the three pulses under investigation. Such a study will help us to understand how exactly the spectral components are depleted as a pulse travels away from the aperture. There have been several serious attempts to set guidelines for the design of LW pulses [6, 7]. To complement these attempts the approach adopted in this work focuses on how the spectral components of the pulses are actually stripped away as they propagate away from the aperture. This gives us a facility to pinpoint the components that need to be retained in order to slow down the decay rate of the pulses generated.

The definition of the diffraction length is a topic that is frequently discussed in connection with the LW generation and propagation [7, 8]. The core of this issue resides in the ambiguity of determining the maximum temporal ($\omega_{\max}$) frequency of the spectrum. Furthermore, the range of the pulse and its rate of decay depend on the transverse spectral bandwidth. These quantities, together with the maximum radius of the aperture, can be combined to give a good estimate of a diffraction length [8]. However, inclusive estimates of this type can conceal some features that might be useful for specific applications.

The reader will probably notice that the parameters used to characterize the generated LW pulses lead to aperture sizes and frequency bandwidths that are slightly exaggerated. The apertures simulated in this work shrink from initial sizes of several metres to minimum radii of few millimetres, while the highest frequencies contained in their spectra are of the order of tens of teraHertz. Such bandwidths are about an order of magnitude larger than those produced by recently developed optical sources [9]. We have chosen such blown up quantities primarily to demonstrate the efficiency of dynamic apertures to launch extremely narrow pulses from extended sources of larger dimensions. For various applications the maximum and minimum radii and the bandwidths of the elements constituting the aperture can be altered according to the design requirements.

In this work we start by deriving three source-free LW solutions. These pulses will be used to illuminate the corresponding dynamic apertures. We continue with a study of the fields generated by apertures that need to be illuminated for infinite periods of time. The Fourier spatial and temporal spectra of these fields are derived and their main features are expounded upon. Next, we concentrate on the physically realizable, finite-time dynamic apertures and show how their spectral components are depleted with distance causing the amplitude of the pulses to decrease. Finally, we provide a discussion of the diffraction length.

2. The source-free solutions

In this section, we utilize the facility provided by the bi-directional representation [10] to derive other source-free solutions that, in analogy to the Gaussian FWM aperture [1], can be used to illuminate similar dynamic apertures. In particular, we suggest three different solutions to the scalar wave equation, namely, the focus wave mode (FWM), the polynomial focus wave mode (PFWM) and the modified focus wave mode (MFWM). At the beginning, these fields will be used to excite infinite dynamic apertures located at $z = 0$. For such ideal sources which will be considered in sections 3 and 4, the aperture shrinks from an infinite radius at $t = -\infty$ to a minimum effective radius at $t = 0$, then expands again to an infinite radius at $t = \infty$. In each case, the initial excitation field will be chosen to produce a forward illumination of the aperture. This excitation field will be defined as a superposition of Bessel beams [11] with a spectrum similar to that of the source-free solutions. The

infinite dynamic apertures [2] are ideal devices that cannot be realized because they need to be illuminated for infinitely long periods of time. However, such a construction will be considered in some detail because it will clarify several subtle aspects related to the performance of the finite-time dynamic apertures.

It has been established that the scalar wave equation

$$(c^{-2}\partial_t^2 - \nabla^2)\Psi(\boldsymbol{r}, t) = 0 \tag{2.1}$$

has the following bi-directional solution [10]:

$$\Psi(\rho, \phi, \xi, \eta) = \frac{1}{(2\pi)^2}\sum_{l=1,-1}\sum_{n=0}^{\infty}\int_0^{\infty}\mathrm{d}\chi\int_0^{\infty}\mathrm{d}(l\alpha)\int_0^{\infty}\mathrm{d}(l\beta)C_n(l\alpha, l\beta, \chi)\chi J_n(\chi\rho)\mathrm{e}^{\pm \mathrm{i}n\phi} \times \mathrm{e}^{-\mathrm{i}l\alpha\xi}\mathrm{e}^{\mathrm{i}\ell\beta\eta}\delta(\alpha\beta - \chi^2/4)$$

where

$$\alpha\beta = \frac{\chi^2}{4} \qquad \eta = z + ct \qquad \xi = z - ct \qquad \text{and} \qquad \frac{\omega}{c} = \beta + \alpha\,. \tag{2.2}$$

The bi-directional superposition [10] given by (2.2) provides the most natural approach for synthesizing Brittingham-like solutions. In the following we shall restrict the discussion to the zeroth order mode ($n = 0$) and ($l = 1$). This is a matter of convenience and it does not affect the generality of the procedure.

We are going to consider three different choices for $C_0(\alpha, \beta, \chi)$. First, we define

$$C_0(\alpha, \beta, \chi) = \frac{\pi}{2}\delta(\beta - \beta')\mathrm{e}^{-\alpha a_1}\,. \tag{2.3}$$

The corresponding source-free solution is the FWM field [4]. Such a field is characterized by a concentration of all the significant temporal and spatial frequency components at the lower end of its spectrum. In later sections, it will be shown within the framework of a finite time excitation of this field that its spectral content is rapidly depleted with distance due to the high oscillations introduced at the low frequency end. The source-free solution is obtained by substituting (2.3) into (2.2) and integrating over α, β and χ to obtain

$$\Psi(\rho, \xi, \eta) = \frac{1}{4\pi(a_1 + \mathrm{i}\xi)}\mathrm{e}^{-\beta'\rho^2/(a_1+\mathrm{i}\xi)}\mathrm{e}^{\mathrm{i}\beta'\eta}\,. \tag{2.4}$$

For the sake of convenience we shall replace, in what follows, β' by β. Another possible choice for $C_0(\alpha, \beta, \chi)$ is

$$C_0(\alpha, \beta, \chi) = \frac{\pi}{2}\delta(\beta - \beta')\chi^6\mathrm{e}^{-\alpha a_1}\,. \tag{2.5}$$

This differs from the spectrum in (2.3) by the χ^6 term, hence, the corresponding source-free solution is the PFWM pulse. It will be shown later on that this solution is characterized by having most of its significant components located at the higher frequency end of its spectrum. Thus, we expect the PFWM pulse, generated by a finite aperture, to decay at a slower rate than the FWM. The source-free solution can be obtained by substituting (2.5) into (2.2) and integrating over α, β and χ. The resulting PFWM pulse is given as

$$\Psi(\rho, \xi, \eta) = \frac{3(4\beta)^4\mathrm{e}^{\mathrm{i}\beta\eta}}{2\pi(a_1 + \mathrm{i}\xi)^4}\left(\frac{1}{6}\left(5 - \frac{\rho^2\beta}{(a_1 + \mathrm{i}\xi)}\right)\left(\frac{\rho^4\beta^2}{(a_1 + \mathrm{i}\xi)^2} - \frac{4\rho^2\beta}{(a_1 + \mathrm{i}\xi)} + 2\right) - \frac{2}{3}\left(1 - \frac{\rho^2\beta}{(a_1 + \mathrm{i}\xi)}\right)\right)\mathrm{e}^{-\beta\rho^2/(a_1+\mathrm{i}\xi)}\,. \tag{2.6}$$

Finally, we choose $C_0(\alpha, \beta, \chi)$ to take the form

$$C_0(\alpha, \beta, \chi) = \frac{\pi}{2}\delta(\beta - \beta')I_0(a_2\chi)\mathrm{e}^{-\alpha a_1} \tag{2.7}$$

where a_2 is a constant and I_0 is the modified Bessel function of the first kind [12]. The corresponding source-free solution is the MFWM field. This solution has low-frequency components that are relatively greater than those of the PFWM but slightly smaller than those of the FWM. The source-free solution is obtained by substituting (2.7) into (2.2) and integrating over α, β and χ; specifically we get

$$\Psi(\rho, \xi, \eta) = \frac{\beta \mathrm{e}^{\mathrm{i}\beta\eta}}{4\pi(a_1 + \mathrm{i}\xi)}\mathrm{e}^{\beta(a_2^2 - \rho^2)/(a_1 + \mathrm{i}\xi)}J_0\left(\frac{2a_2\rho\beta}{a_1 + \mathrm{i}\xi}\right). \tag{2.8}$$

It has been shown in a previous work [2] that the source-free FWM solution can be represented as a superposition of forward and backward propagating components. In order to efficiently produce a causal FWM pulse dominated by outgoing propagating components, we must choose $\beta a_1 \ll 1$. For the other two cases, namely the PFWM and the MFWM, the same condition ensures that the radiated fields are dominated by the forward propagating components. A reasonable selection is to take $\beta = 1.25\ \mathrm{m}^{-1}$ and $a_1 = 0.000\,01$ m throughout this work.

3. The Fourier spectra of the illuminations of three infinite dynamic apertures

In this section we consider three different cases for initially exciting an infinite dynamic aperture located at $z = 0$. In each case, the initial field will be chosen to have the same Fourier spectrum as that of the source-free solution derived in the preceding section. Consequently, we need to calculate the Fourier spectra for the three source-free solutions, given by (2.4), (2.6) and (2.8), at $z = 0$. For an azimuthally symmetric wavefield, the Fourier spectrum of the initial excitation is defined as

$$\Phi(\chi, \omega) = \int_{-\infty}^{+\infty}\mathrm{d}t\int_0^{\infty}\mathrm{d}\rho\,\rho J_0(\chi\rho)\mathrm{e}^{-\mathrm{i}\omega t}\Psi(\rho, 0, t) \tag{3.1}$$

where $\chi = \sqrt{k_x^2 + k_y^2}$ is the transverse component of the wavevector. By substituting (2.4) into (3.1), setting $z = 0$ and integrating over ρ and t, we get the Fourier spectrum of the FWM which is given explicitly as

$$\Phi(\chi, \omega) = \frac{1}{4c\beta}\mathrm{e}^{-\chi^2 a_1/4\beta}\delta((\chi^2/4\beta) + \beta - \omega/c)\,. \tag{3.2}$$

Similarly, we substitute (2.6) into (3.1) and set $z = 0$. The double integration over t and ρ yields the Fourier spectrum of the PFWM; specifically,

$$\Phi(\chi, \omega) = \frac{1}{4c\beta}\chi^6\mathrm{e}^{-\chi^2 a_1/4\beta}\delta((\chi^2/4\beta) + \beta - \omega/c)\,. \tag{3.3}$$

Along the same vein, the substitution of (2.8) into (3.1) at $z = 0$ produces the MFWM Fourier spectrum, namely

$$\Phi(\chi, \omega) = \frac{1}{4c\beta}I_0(a_2\chi)\mathrm{e}^{-\chi^2 a_1/4\beta}\delta((\chi^2/4\beta) + \beta - \omega/c)\,. \tag{3.4}$$

The initial illumination of the aperture utilizes a wide-band field whose temporal and spatial frequency contents are coupled together through the argument of the delta function appearing in (3.2)–(3.4). Such a coupling does not exist for quasi-monochromatic continuous wave (CW) excitations. Also, we do not have a specific carrier frequency to resort to in

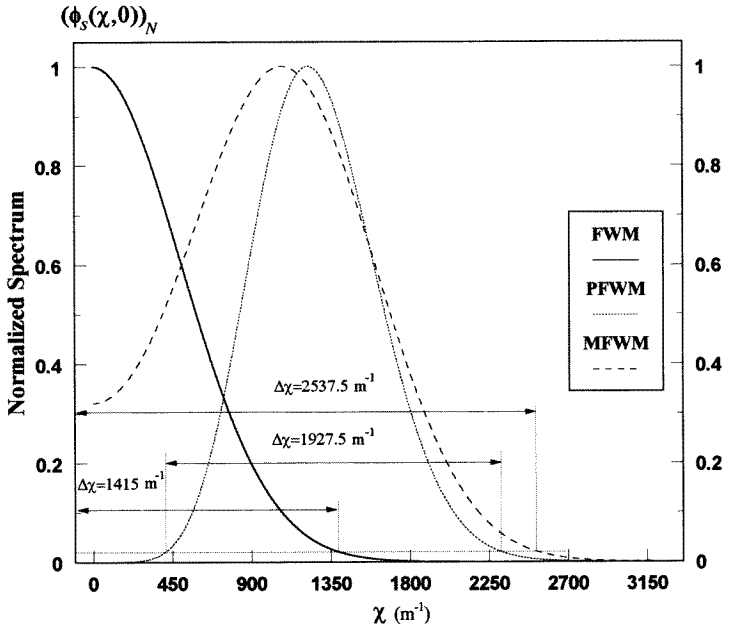

Figure 1. The spatial spectrum of an infinite-dynamic aperture when initially illuminated by the FWM, PFWM or MFWM fields.

calculating the diffraction length as in the case of CW. As a consequence, we have to set a criterion for specifying the maximum frequency components for the temporal and spatial spectra. We choose to define the maximum frequency as that at which the spectrum amplitude drops to $(1/e^4)$ of its maximum value. This is quite a severe condition and has been adopted to take the effects of the extended tails into consideration.

In what follows we need to differentiate between the spatial and temporal spectral contents. At $t = 0$, the former contains the Fourier information concerning the spatial distribution of the focused illumination of the aperture. We start by defining the spatial spectrum as

$$\Phi_s(\chi, t) = \frac{1}{2\pi}\int_{-\infty}^{+\infty} d\omega\, \Phi(\chi, \omega) e^{i\omega t}. \tag{3.5}$$

The spatial spectra of the three cases under consideration are obtained by substituting (3.2)–(3.4) into (3.5) to give

$$\Phi_s(\chi, t) = \frac{f(\chi)}{8\pi\beta} e^{-\chi^2 a_1/4\beta} e^{i((\chi^2 a_1/4\beta)+\beta)ct} \tag{3.6}$$

where $f(\chi)$ is equal to 1, χ^6 and $I_0(a_2\chi)$, for the cases of the FWM, PFWM and MFWM, respectively. The full curve in figure 1 displays the shape of $\Phi_s(\chi, 0)$ characterizing the FWM pulse. From this figure it is clear that most of the significant components of the χ-spectrum are concentrated at its lower end. It will be shown that, for a finite-time aperture (cf section 5) this causes the centroid of the pulse to decay quickly as the pulse propagates away from the aperture. From figure 1 it is also clear that the bandwidth of the FWM spatial spectrum is $\Delta\chi = 1415\ \text{m}^{-1}$. Notice that the bandwidth of the spatial spectrum of the FWM initial pulse is controlled by the second exponential term on the right-hand side

of (3.6). The $(1/e^4)$ point of such a term determines $\chi_{max} = 4\sqrt{\beta/a_1} = 1415\ m^{-1}$. The FWM maximum spatial frequency is smaller than that of the PFWM and MFWM pulses because their spectra contain the term $f(\chi)$ which equals χ^6 or $I_0(a_2\chi)$, respectively. If we refer to the dotted curve in figure 1, we notice that the χ-spectrum of the PFWM at $t = 0$ is characterized by having significant components at higher values than those of the FWM spatial spectrum. Such a difference in the shape of the spatial spectrum allows the PFWM pulse, generated by a finite-time aperture, to hold together for larger distances before its centroid starts to decay. A detailed analysis of this point will be provided in section 5. The bandwidth of the PFWM spatial spectrum is measured as the χ difference between the two points at which the amplitude is $(1/e^4)$ of its maximum value. From figure 1 it is clear that $\Delta\chi = 1927.5\ m^{-1}$. Finally, the broken curve in figure 1 represents the spatial spectrum of the MFWM pulse. It should be noted that this case is an intermediate choice between the FWM and PFWM. We notice, however, that the tails of the MFWM spectrum decay more slowly than those of the PFWM due to the presence of the $I_0(a_2\chi)$ term which increases exponentially for large values of $(a_2\chi)$ [12]. The value of a_2 was adjusted so that the peak value of the MFWM spatial spectrum is as near as possible to that of the PFWM. At the same time the tails of both spectra were kept close to each other for future comparison between the two cases. A reasonable value of a_2 is taken to be 0.0048 m. From figure 1, it is clear that the bandwidth of the MFWM spatial spectrum is $\Delta\chi = 2537.5\ m^{-1}$.

The spectra given in (3.2)–(3.4) indicate that the temporal frequency ω is closely related to the spatial frequency χ through the delta function $\delta((\chi^2/4\beta)+\beta-\omega/c)$. Specifically, we define the temporal frequency content of the dynamic apertures, whose illumination fields have the spectra (3.2)–(3.4), as follows:

$$\Phi_t(\rho,\omega) = \int_0^\infty d\chi\ \chi J_0(\chi\rho)\Phi(\chi,\omega)\,. \tag{3.7}$$

The temporal spectra of the FWM, the PFWM and the MFWM are obtained by substituting their corresponding $\Phi(\chi,\omega)$ Fourier components into (3.7) to give

$$\Phi_t(\rho,\omega) = \frac{g(\omega)}{2c} J_0(2\sqrt{\beta((\omega/c)-\beta)}\rho)e^{-a_1((\omega/c)-\beta)} H_s((\omega/c)-\beta) \tag{3.8}$$

where $H_s((\omega/c)-\beta)$ is the Heaviside unit step function. For the FWM field $g(\omega) = a_1$. The full curve in figure 2 shows $\Phi_t(0,\omega)$ associated with the FWM pulse. We notice from this curve that the temporal spectrum of the FWM resembles to a great extent the spatial spectrum. This is the case because $\omega/c = (\chi^2/4\beta)+\beta$. The temporal spectrum has most of its significant components concentrated at the low frequency end of the spectrum. The bandwidth is again defined as the range for which all spectral amplitudes are larger than $(1/e^4)$ of the maximum value of the spectrum. By inspection, figure 2 shows that the maximum frequency component is $f_{max} = 19.1$ THz. The same value could be derived directly by noting that the $e^{-\omega a_1}$ term in (3.8) determines the bandwidth of the temporal spectrum; specifically, $\omega_{max} = 4/a_1$. The dotted curve of figure 2 represents the temporal spectrum of the PFWM that has $g(\omega) = (4\beta)^3(\omega/c-\beta)^3$. It can be shown in this case that the maximum frequency component is $f_{max} = 51.85$ THz. It is clear that the bandwidth of the PFWM is larger than that of the FWM case. For the case of the MFWM we have $g(\omega) = I_0(2a_2\sqrt{\beta(\omega/c-\beta)})$. Referring to the broken curve in figure 2, we note that this temporal spectrum is again intermediate between those of the FWM and PFWM. The bandwidth in this case is $f_{max} = 61.56$ THz. This value is larger than that of the PFWM as the tails of the MFWM spectrum roll off at slightly slower rate than those of the PFWM spectrum. Notice that the latter two spectra show a great resemblance to their corresponding spatial spectra.

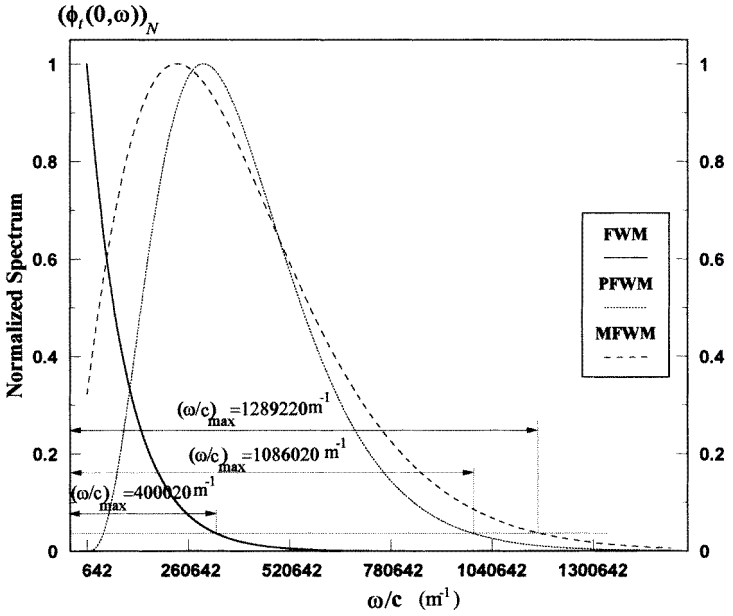

Figure 2. The temporal spectrum of an infinite-dynamic aperture when initially illuminated by the FWM, PFWM or MFWM fields.

The case of the infinite dynamic aperture has been considered in detail in another paper [2]. It has been shown that such a source is capable of launching a causal localized pulse that closely resembles the source-free FWM pulse. The generated pulse propagates with no dispersion at all because the aperture is allowed to expand to an infinite size. Similar apertures can be postulated for the PFWM and MFWM cases, and the same dispersion-free propagation is anticipated for the generated pulses. The shapes of the corresponding spectra do not affect the fields generated from the infinite apertures because they produce fields that propagate without any dispersion. However, they have direct impact when finite dynamic apertures are considered. The position of the significant spectral components and the roll off of the tails have a decisive effect on the range at which the centroids of the generated pulses start to decay and the rate of the decay.

4. The field propagating in the $z > 0$ half-space

The initial field defined on the aperture is a superposition of Bessel beams [11] on the plane $z = 0$; specifically,

$$\Psi_i(\rho, t) = \Re\left(\frac{1}{2\pi}\int_0^\infty \mathrm{d}\chi\ \chi J_0(\chi\rho)\int_0^\infty \mathrm{d}\omega\ \Phi(\chi,\omega)\mathrm{e}^{-\mathrm{i}(\sqrt{(\omega/c)^2-\chi^2})z}\mathrm{e}^{\mathrm{i}\omega t}\right)_{z=0}. \tag{4.1}$$

The normal derivative of the field on the aperture is derived by taking the derivative of the above expression with respect to z before we set $z = 0$. Consequently, the quantity $\sqrt{(\omega/c)^2 - \chi^2}$ is restricted to positive values to ensure a forward illumination of the aperture. Notice, also, that ω is restricted to positive values if β is positive. This follows from the roots of the δ-function in the spectra given in (3.2)–(3.4).

When any one of the spectra given in (3.2)–(3.4) is substituted in (4.1) we obtain an initial field that has the form of the corresponding source-free solution (cf equations (2.4),

(2.6) and (2.8), but with $z = 0$). Because of the exponential term $e^{-\beta\rho^2/(a_1 - ict)}$ in the three fields under consideration, the resulting illumination appears to have an effective radius that varies with time. Equivalently we have an aperture whose size varies with time. For $\beta a_1 \ll 1$, the aperture apparently shrinks and expands monotonically at speeds greater than that of light. This can be achieved by utilizing independently addressable aperture elements [13, 14].

To calculate the outgoing field propagating into the $z > 0$ half space, the Huygen's construction [15] is applied to the initial excitation of the aperture. Accordingly, the field at a point $\boldsymbol{R}$ and time t inside a wavefront surface (being zero outside such a surface) is given by the following integration over the area of the infinite aperture:

$$\Psi(\rho, z, t) = \frac{1}{4\pi}\int_0^{2\pi} d\phi' \int_0^{\infty} d\rho' \frac{\rho'}{R}\left(-\partial_{z'}\Psi(\rho', z' = 0, t') + \frac{z}{R^2}\Psi(\rho', z' = 0, t') + \frac{z}{Rc}\partial_{t'}\Psi(\rho', z' = 0, t')\right)_{t'=t} - R'/c \tag{4.2}$$

where $R = \sqrt{\rho'^2 + \rho^2 - 2\rho'\rho\cos\phi' + z^2}$. The primed coordinates refer to source points on the aperture, while the unprimed ones refer to the observation points n the $z > 0$ half space. The substitution of the initial field (4.1) into (4.2) yields

$$\Psi(\rho, z, t) = \Re(\hat{\Psi}(\rho, z, t)) \tag{4.3a}$$

where

$$\hat{\Psi}(\rho, z, t) = \frac{1}{2\pi}\int_0^{\infty} d\chi\ \chi J_0(\chi\rho)\int_0^{\infty} d\omega\ \Phi(\chi, \omega)e^{i\omega t}e^{-i(\sqrt{(\omega/c)^2 - \chi^2})z}. \tag{4.3b}$$

In the case of the FWM, the initial field exciting the aperture is obtained by substituting (3.2) into (4.1). The field propagating in the $z > 0$ half-space, due to this initial excitation, is obtained by substituting (3.2) into (4.3*b*). Explicitly, we have

$$\hat{\Psi}(\rho, z, t) = \frac{1}{8\pi c\beta}\int_0^{\infty} d\chi\ \chi J_0(\chi\rho)\int_0^{\infty} d\omega\ e^{i\omega t}e^{-\chi^2 a_1/4\beta}\delta((\chi^2/4\beta) + \beta - \omega/c) \times e^{-i(\sqrt{(\omega/c)^2 - \chi^2})z}. \tag{4.4}$$

The above expression is the same as the source-free solution except that the quantity $\sqrt{(\omega/c)^2 - \chi^2}$ acquires only positive values [1, 2]. Hence for $\omega/c = (\chi^2/4\beta) + \beta$ the square root $\sqrt{(\omega/c)^2 - \chi^2}$ acquires either the value $((\chi^2/4\beta) - \beta)$ or $-((\chi^2/4\beta) - \beta)$, depending on whether $\chi > 2\beta$ or $\chi < 2\beta$, respectively. This is the case because only positive values of the square root give non-zero contributions to the outgoing radiated field [1, 2]. One can, then, carry out the integration over ω to obtain

$$\hat{\Psi}(\rho, z, t) = \frac{i}{4\pi\beta}\int_0^{2\beta} d\chi\ \chi J_0(\chi\rho)e^{-\chi^2 a_1/4\beta}\sin(((\chi^2/4\beta) - \beta)z)e^{i(\chi^2/4\beta + \beta)ct} + \frac{1}{8\pi\beta}\int_0^{\infty} d\chi\ \chi J_0(\chi\rho)e^{-\chi^2 a_1/4\beta}e^{i(\chi^2/4\beta)(z - ct)}e^{-i\beta(z + ct)}. \tag{4.5}$$

For $\beta a_1 \ll 1$, most of the significant χ-spectral components exist at values greater than 2β [1, 2, 10]. Hence, the first term on the right-hand side of the above equation is of $O(\beta a_1)$ relative to the second term. It only contributes significantly away from the centroid of the pulse. The same conclusion can be directly reached by referring to the full curve in figure 1. For $\beta = 1.25\ m^{-1}$, the first integration represents a negligible portion of the χ-spectrum compared to the second one. The integration of the second term on the right-hand side of

(4.5) yields the source-free FWM pulse. Thus, integrating (4.5) after neglecting the first term we get for the radiated field,

$$\hat{\Psi}(\rho, z, t) \cong \frac{1}{4\pi(a_1 + \mathrm{i}(z - ct))} \mathrm{e}^{-\beta\rho^2/(a_1+\mathrm{i}(z-ct))} \mathrm{e}^{\mathrm{i}\beta(z+ct)} \tag{4.6}$$

which is approximately the same as the FWM source-free solution. Similarly, we use the spectra of the PFWM and the MFWM to define the initial excitation of the aperture (4.1). It can then be shown that the fields propagating in the $z > 0$ half-space are approximations to the corresponding source-free solutions.

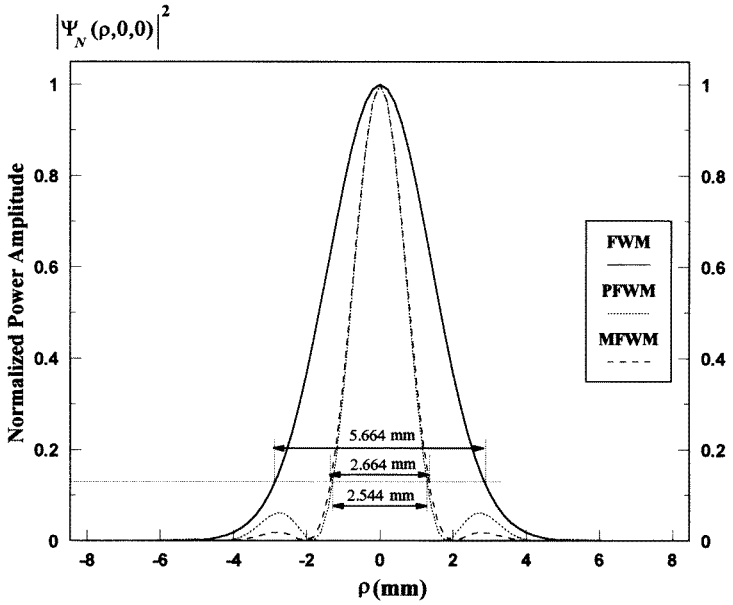

Figure 3. The power content of the FWM, PFWM and MFWM central pulses on the aperture at $z = ct = 0$.

The infinite-dynamic apertures have radii that shrink from infinity to their minimum effective values before they expand once more to infinity [2]. The minimum effective radius of the aperture is the same as that of the generated central pulse. In what follows, we choose to define the minimum effective radius of the infinite-dynamic aperture as the radius at which the value of the power content of the field at $z = ct = 0$ drops to $(1/\mathrm{e}^2)$ of its peak value. Figure 3 represents the power of the field on the aperture when it shrinks to its smallest size (at $z = ct = 0$). The three illuminating fields under consideration are shown. The full curve displays the FWM excitation, the dotted one gives the PFWM excitation and the broken curve represents the MFWM case. Comparing these three curves we notice that the power of the FWM pulse is distributed over a greater radius than that of both the PFWM and MFWM pulses. This should be expected because it has a smaller spatial frequency bandwidth. A comparison of the PFWM pulse to the MFWM shows that these two pulses are nearly identical up to $\rho = 1.6$ mm. Beyond this value we notice that the power content in the secondary lobe of the PFWM pulse is greater than that in the MFWM pulse. From the figure it is also clear that the minimum effective radius of the FWM pulse is $R_{\min} = 2.83$ mm while that of the PFWM is $R_{\min} = 1.272$ mm and that of the MFWM is $R_{\min} = 1.33$ mm. This shows that the minimum effective radii of the PFWM and MFWM

are almost equal to each other and that both are about half the radius of the FWM pulse. It is worthwhile to point out that decent estimates of the minimum effective radii can be deduced as the reciprocals of the maximum spatial frequencies, specifically, $R_{\min} \cong 4/\chi_{\max}$. This expression is especially accurate for the case of the FWM, for which $R_{\min} = \sqrt{a_1/\beta}$, because of its Gaussian transverse radial dependence and because corresponding spatial spectrum is also Gaussian.

5. The finite-time excitation of the dynamic apertures

The field generated from an infinite dynamic aperture propagates in the $z > 0$ half-space without any decay. Such a scheme suffers from the disadvantage of using an aperture of infinite size. Moreover, the aperture needs an infinite amount of energy as the illumination field must exist for an infinite period of time. Thus, a practical realization of such an aperture is impossible. In this section, we try to circumvent the aforementioned shortcomings by using a dynamic aperture which is illuminated for a finite period of time. This can be realized by applying a Gaussian time window to the initial infinite-time excitations discussed in the preceding sections. The finite-time dynamic aperture utilizes a finite amount of energy. Moreover, it expands to a maximum radius of a finite extension. In return, the generated pulse starts decaying after it travels a certain distance away from the aperture. In the following sections we define the initial excitations of this aperture, calculate their Fourier spatial and temporal spectra and determine the decay rate of the fields propagating in the $z > 0$ half-space.

In order to investigate the consequences of cutting off the expansion time of the dynamic aperture at a finite value, we introduce a Gaussian time window having a span of $8T$, which is explicitly given by $\mathrm{e}^{-t^2/4T^2}$. By cutting off the illumination of the aperture at $t = -4T$ and $t = +4T$, we allow it to start shrinking from a finite initial size, to reach its minimum extension, then to expand back to the same original finite radius. It should be emphasized, however, that such a scheme differs from having an aperture of a finite physical size excited for a finite period of time $|t| < 4T$. The values of T chosen henceforth yield the same maximum radii for the three cases under consideration. Specifically, we choose $cT = 6.25$ mm for the FWM, and $cT = 2.5$ mm for both the PFWM and MFWM. The reasons for such choices are given in section 6. At this point, the reader should recognize that the longitudinal extensions of the LW fields investigated are equal to $8cT$ and is much larger the length of the highly focused central portion of the pulse which is of order $\mathrm{O}(a_1)$.

First we shall consider the case of the FWM. The spectral content of the FWM initial excitation is calculated as follows:

$$\Phi(\chi, \omega) = \int_{-\infty}^{+\infty} \mathrm{d}t \int_0^{\infty} \mathrm{d}\rho\, \rho J_0(\chi\rho) \mathrm{e}^{-\mathrm{i}\omega t} \frac{\mathrm{e}^{-\beta\rho^2/(a_1 - \mathrm{i}ct)}}{4\pi(a_1 - \mathrm{i}ct)} \mathrm{e}^{\mathrm{i}\beta ct} \mathrm{e}^{-t^2/4T^2}. \tag{5.1}$$

Here, the Gaussian time window allows the aperture to expand only from $t = -4T$ to $+4T$. Integrating equation (5.1) over ρ and t, the spectrum illuminating the aperture becomes

$$\Phi(\chi, \omega) = \frac{1}{4\beta c} \hat{\delta}\left(\frac{\omega}{c} - ((\chi^2/4\beta) + \beta); cT\right) \mathrm{e}^{-\chi^2 a_1/4\beta} \tag{5.2}$$

where

$$\hat{\delta}\left(\frac{\omega}{c} - ((\chi^2/4\beta) + \beta); cT\right) = \frac{cT}{\sqrt{\pi}} \mathrm{e}^{-(cT)^2((\omega/c) - ((\chi^2/4\beta) + \beta))^2}. \tag{5.3}$$

Similarly, we can deduce the finite-time Fourier content for the other two cases. This yields expressions analogous to (3.3) and (3.4) with the Gaussian function $\hat{\delta}((\omega/c) -$

$((\chi^2/4\beta)+\beta);cT)$ replacing the Dirac delta function $\delta((\chi^2/4\beta)+\beta-\omega/c)$. In the limit as $T\to\infty$, the Gaussian $\hat{\delta}$-function goes to the Dirac δ-function characterizing the spectrum of the infinite-time excitation. When cT is large, the Gaussian in the spectrum of the FWM, PFWM and MFWM reduces to a narrow distribution with a small bandwidth $\eta(\omega)\sim \mathrm{O}(2\pi/T)$, for which $\omega/c\sim((\chi^2/4\beta)+\beta)$. Such a narrow frequency window varies with χ and provides most of the significant contributions to the amplitude of the centroid of the pulse.

To clarify these issues, let us consider the temporal spectrum of the finite-time FWM excitation, which is given explicitly by

$$\Phi_t(\rho,\omega)=\frac{T}{4\sqrt{\pi}\beta}\int_0^\infty \mathrm{d}\chi\ \chi J_0(\chi\rho)\mathrm{e}^{-\chi^2 a_1/4\beta}\mathrm{e}^{-(cT)^2(\chi^2/4\beta+\beta-\omega/c)^2}. \tag{5.4}$$

In this case, for each value of ω, the significant contributions of the integrand results from varying χ from $\sqrt{4\beta((\omega/c)+\beta-(4/cT))}$ to $\sqrt{4\beta((\omega/c)+\beta+(4/cT))}$. If we examine this range we notice that for relatively high values of χ and T, the limiting values in the range of χ represent very small deviations around $\sqrt{4\beta((\omega/c)+\beta)}$. Hence, most of the contributions to the integration come from $\chi\cong\sqrt{4\beta((\omega/c)+\beta)}$. This means the temporal spectrum of the finite excitation closely resembles that of the infinite illumination case. In fact, a direct evaluation of (5.4) gives a temporal spectrum which is indistinguishable from that of the infinite-time excitation given in figure 2. For all practical purposes, we can consider the finite-time excitation to have a temporal spectrum which is very close to that of the infinite-time case. Using the same analysis we can show that the spatial spectrum of the finite-time excitation has the same form and bandwidth as that of the infinite-time illumination. The same results are valid also for both the PFWM and the MFWM pulses.

To deduce the shape of the field propagating in the $z>0$ half-space, we follow an analysis analogous to that used for the case of the infinite aperture. For the case of the FWM, the initial field exciting the aperture has the same spectrum as that of the finite-time FWM spectrum and is given explicitly as

$$\Psi_i(\rho,t)=\Re\left(\frac{1}{8\pi\beta c}\int_0^\infty \mathrm{d}\chi\ \chi J_0(\chi\rho)\int_0^\infty \mathrm{d}\omega\,\mathrm{e}^{-\chi^2 a_1/4\beta}\hat{\delta}((\omega/c)-((\chi^2/4\beta)+\beta);cT)\right.$$
$$\left.\times\mathrm{e}^{\mathrm{i}\omega t}\mathrm{e}^{-\mathrm{i}(\sqrt{(\omega/c)^2-\chi^2})z}\right)_{z=0}. \tag{5.5}$$

The field propagating in the $z>0$ half-space, due to this initial excitation, is calculated by substituting (5.2) into (4.3) to obtain

$$\Psi(\rho,z,t)=\frac{1}{8\pi\beta c}\int_0^\infty \mathrm{d}\chi\ \chi J_0(\chi\rho)\int_0^\infty \mathrm{d}\omega\mathrm{e}^{-\chi^2 a_1/4\beta}\hat{\delta}((\omega/c)-((\chi^2/4\beta)+\beta);cT)$$
$$\times\cos(\omega t-(\sqrt{(\omega/c)^2-\chi^2})z). \tag{5.6}$$

In analogy to the infinite-time excitation, the square root $\sqrt{(\omega/c)^2-\chi^2}$ acquires only positive values to ensure that all the field components are propagating away from the aperture. To study the decay pattern of the field given in (5.6), we shall concentrate on the centroid of the pulse at $z=ct$ for $t>0$. The integration given in (5.6) is evaluated numerically. As z increases, the integrand can become highly oscillatory. This leads to some difficulty in calculating the double integration (5.6). However, the numerical job can be reduced significantly if the narrowness of the window is taken into consideration. In particular, one should note that for the field generated from an infinite dynamic aperture, the Dirac δ-function in the spectrum forces the phase $((\omega/c)-\sqrt{(\omega/c)^2-\chi^2})z=2\beta z$ to be independent of χ. Hence the centroid propagates to infinite distances from the aperture

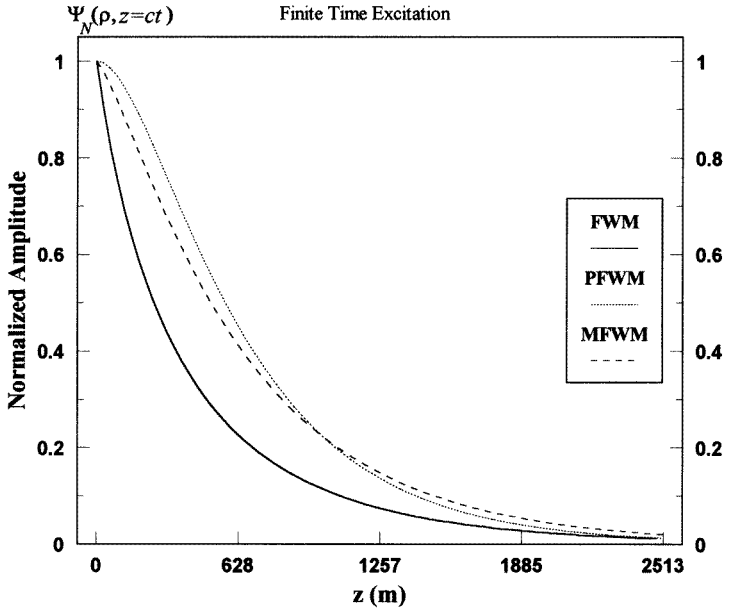

Figure 4. The decay of the centroid of the FWM, PFWM and MFWM pulses radiated from a finite-dynamic aperture.

without any decay and only varies sinusoidally over distances that are integral multiples of π/β. Now, for the finite aperture such a delicate balance does not exist. Even though the phase $\left((\omega/c)-\sqrt{(\omega/c)^2-\chi^2}\right)z \sim 2\beta z$, the Gaussian $\hat{\delta}$-function introduces small deviations that are dependent on both χ and z. These deviations introduce oscillations into the integrand that increase with the distance z. Hence, as the pulse travels to larger distances away from the aperture, the integration in (5.6) yields smaller field amplitudes. At this point we would like to point out that the Gaussian $\hat{\delta}((\omega/c) - ((\chi^2/4\beta) + \beta); cT)$ becomes very narrow in comparison to the total bandwidth for $cT \gg a_1$. Therefore, instead of having an infinite range of integration over ω we effectively have a finite range that we have chosen to vary from $[(\chi^2/4\beta) + \beta - (4/cT)]$ to $[(\chi^2/4\beta) + \beta + (4/cT)]$. All the significant contributions come from this finite ω-window. Subsequently, the computation of the double integration is greatly simplified. Figure 4 represents the decay of the centroid of the field propagating in the $z > 0$ half-space, for the three cases under consideration. In the range investigated, the amplitudes of the centroids vary sinusoidally with distance. Two consecutive peaks are separated by a distance equal to π/β. The figure shows only the field amplitude at those peaks. From the figure, we notice that near the aperture, the FWM field (cf the full curve) decays rapidly with distance, which is expected because most of the significant components of its χ-spectrum lie at low values of χ. Furthermore, oscillations introduced with distance appear first at those low frequency values. On the other hand, both PFWM and MFWM hold for longer distances with the PFWM field performing better than the MFWM field up to $z \cong 1$ km. This is the case because the PFWM field does not have any significant low χ-spectrum components. As z exceeds 1 km the MFWM field starts to overtake the PFWM field because the tails of the χ-spectrum of the MFWM field roll off at a slower rate than that of the PFWM.

The decay of the central portion of the pulse at $z = ct$ with distance is demonstrated

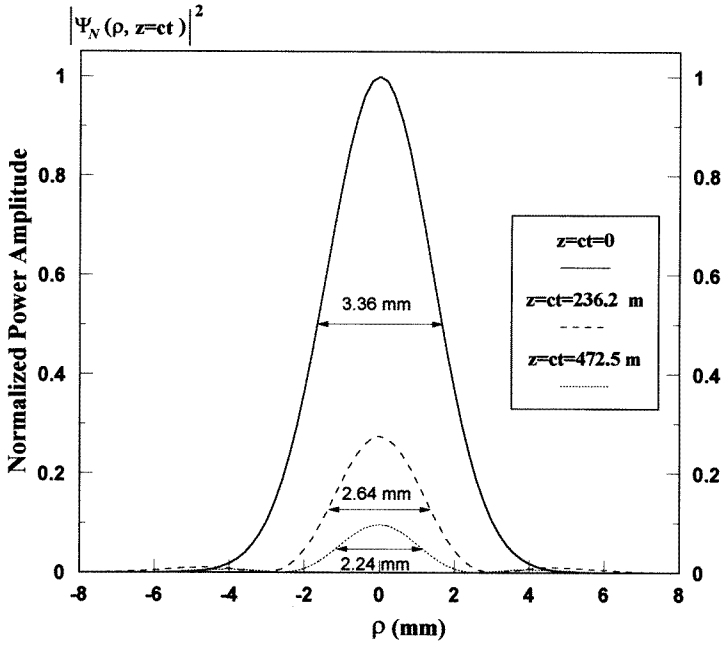

Figure 5. The power content of the FWM central pulse at $z = 0$, 236.2 and 472.5 m.

by plotting the field propagating away from the aperture at certain values of z. The power amplitude of the central pulse at the aperture (i.e. at $z = ct = 0$) has the same distribution as the case of the infinite-time excitation. As the pulse propagates away from the aperture the power in the FWM pulse decays with distance as shown in figure 5. The normalized power amplitude of the pulse is plotted at different values of z. From the figure, we notice that the width of the central pulse decreases with distance, as the half power width for $z = 0$, 236.2, 472.5 m gives the waist $w = 2\rho = 3.36$, 2.64, 2.24 mm, respectively. For both the PFWM and MFWM fields the power amplitude of the central pulse is plotted for specific z values in figures 6 and 7, respectively. The rate of decay of their power amplitude with distance is initially smaller than that of the FWM pulse. We notice also that both pulses are narrower than the FWM pulse for the selected values of z. The MFWM central pulse decays initially faster than the PFWM, but at farther distances the MFWM field holds better than the PFWM.

To enhance our understanding of how the amplitude of the pulse decreases with distance, we demonstrate how the spatial spectrum components are depleted as the pulse travels away from the aperture. To do this we need to consider the spatial spectrum at any distance z from the aperture; the latter is defined as

$$\Phi_s(\chi, z, t) = \frac{1}{2\pi}\int_0^\infty d\omega\, \Phi(\chi, \omega)\cos((\sqrt{(\omega/c)^2 - \chi^2})z - \omega t)\,. \tag{5.7}$$

The spatial spectrum of the FWM at any distance z from the aperture is given by substituting (5.2) into (5.7) to give

$$\Phi_s(\chi, z, t) = \frac{T\, e^{-\chi^2 a_1/4\beta}}{8\pi\sqrt{\pi}\,\beta}\int_0^\infty d\omega\, e^{-(cT)^2((\chi^2/4\beta)+\beta-\omega/c)^2}\cos((\sqrt{(\omega/c)^2 - \chi^2})z - \omega t)\,. \tag{5.8}$$

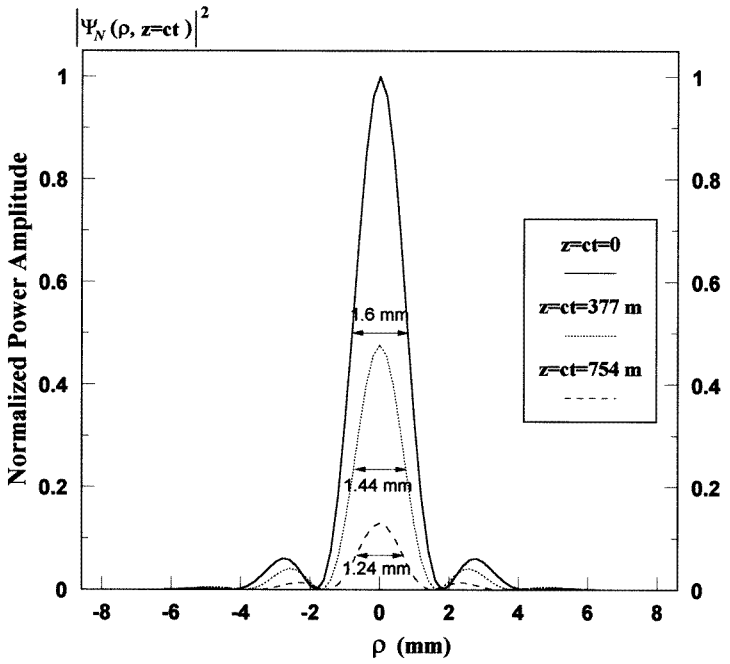

Figure 6. The power content of the PFWM central pulse at $z = 0$, 377 and 754 m.

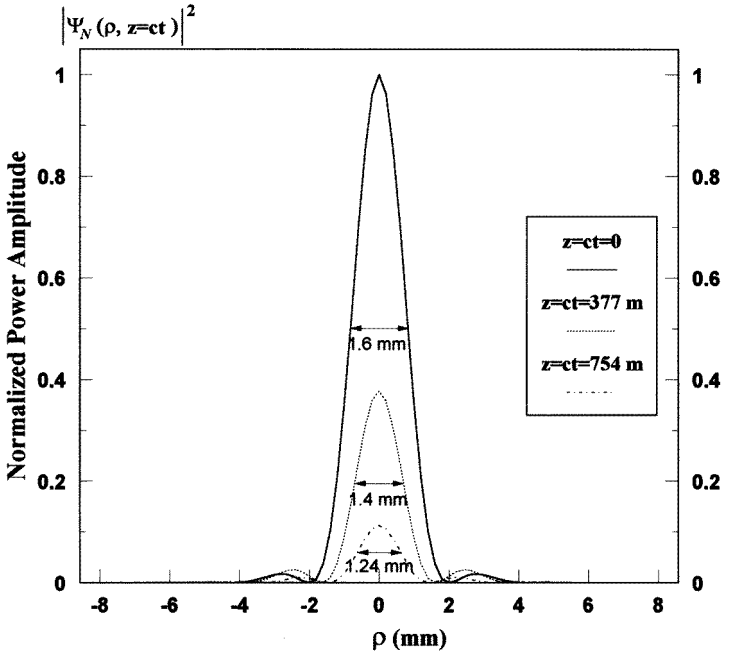

Figure 7. The power content of the MFWM central pulse at $z = 0$, 377 and 754 m.

The integration in (5.8) is evaluated numerically at different values of z and the results

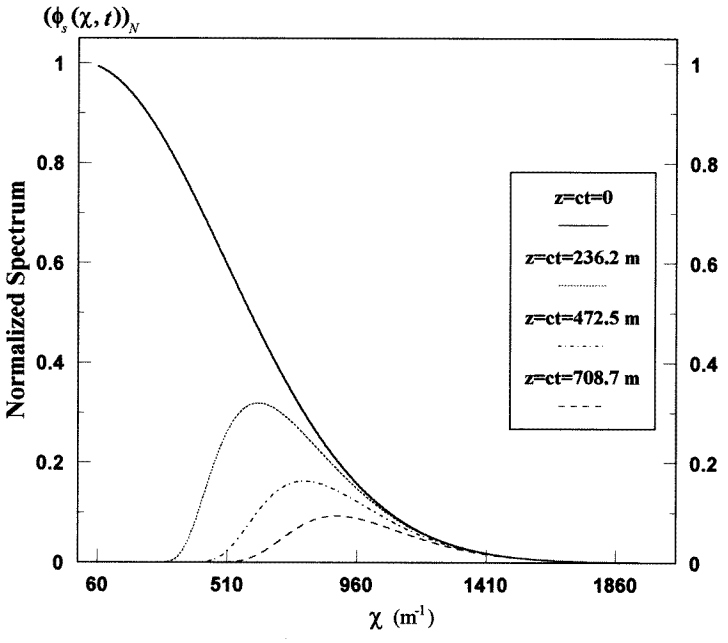

Figure 8. The FWM spatial spectrum at $z = 0$, 236.2, 472.5 and 708.7 m.

are plotted in figure 8. From this figure, it is clear that the χ-spectrum decays rapidly with distance due to the high oscillations introduced at low values of χ. Next, we consider the spatial spectrum of the PFWM and MFWM that are derived by substituting the corresponding $\Phi(\chi, \omega)$ spectra into (5.7). The depletion of their spatial spectra are shown in figures 9 and 10.

The main factor affecting the decay of the centre of the pulse ($z = ct$) or the depletion of the spatial spectrum is the oscillations inside the spectral window,

$$\xi(\chi, \omega) = \mathrm{e}^{-(cT)^2((\chi^2/4\beta)+\beta-\omega/c)^2} \cos(\sqrt{(\omega/c)^2 - \chi^2} - \omega/c)z \,. \tag{5.9}$$

These oscillations depend on the values of χ and z. For the same value of z, the oscillations are decreased as χ increases. On the other hand, for the same value of χ, the oscillations are increased as z increases. Equation (5.9) is plotted in the insets of figure 11 for sampled values of χ, at $z = 784.1$ m and $cT = 6.25$ mm. We observe from this figure that the oscillations inside the ω-window are high for low values of χ. Hence, the net area under the $\xi(\chi, \omega)$ curve is nearly zero. As χ increases, the oscillations decrease and the area starts to increase gradually. This means that if the spatial spectrum has significant components at small values of χ, then a large portion of the spectrum will be quickly depleted with distance. This effect is shown in the main part of the plot, where $\chi\phi_s(\chi, z = ct)$ of the FWM pulse is evaluated at $z = 784.1$ m and is compared to $\chi\phi_s(\chi, z = ct = 0)$. Consequently, the field propagating away from the aperture will decay with distance. In figure 11, we should also note that the ω-window has a bandwidth $\eta(\chi)$ must smaller than that of the total temporal width. This is the case because $\eta(\omega) \sim \mathrm{O}(2\pi/T)$ is very small compared to the total bandwidth $\Delta(\omega) \sim \mathrm{O}(c/a_1)$. However, the ω-windows in the insets are plotted with a scale that differs than that of the χ-spectrum, so we can fit the four of them together.

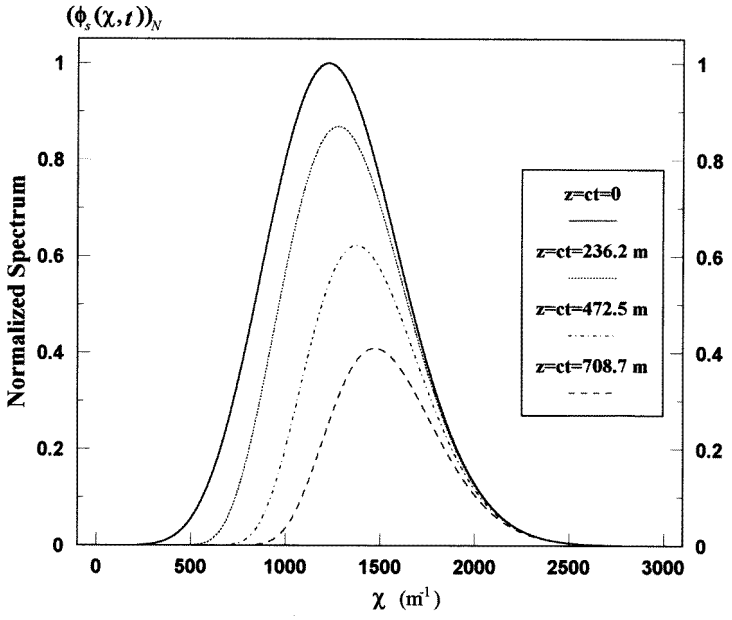

Figure 9. The PFWM spatial spectrum at $z = 0$, 236.2, 472.5, 708.7 m.

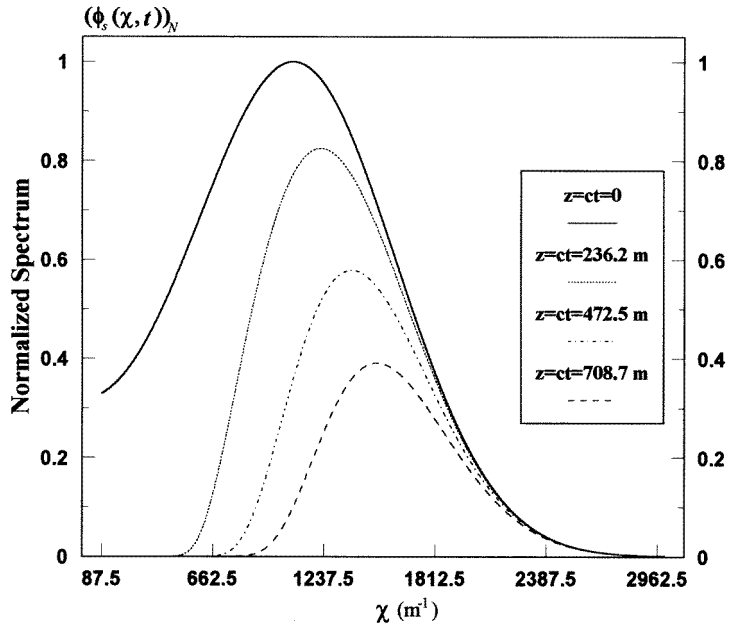

Figure 10. The MFWM spatial spectrum at $z = 0$, 236.2, 472.5, 708.7 m.

6. The diffraction length of the finite dynamic aperture

There have been several attempts to estimate the diffraction length of localized wave solutions generated from apertures driven from sources having ultra-wide frequency

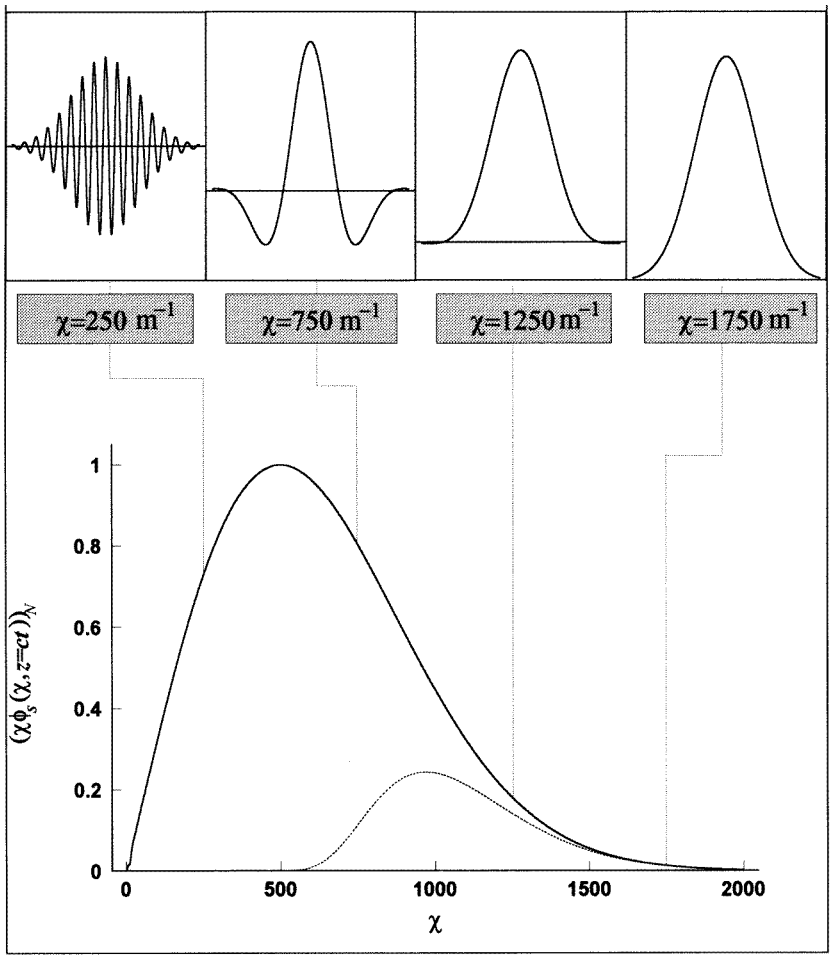

Figure 11. Oscillations affecting different sections of the FWM spatial spectrum at $z = ct = 784.1$ m.

bandwidths. The usual definition of the near-far field limit depends on the size of the aperture and the frequency of the source; specifically the Rayleigh limit is usually defined as $\pi R^2/\lambda$, where R is the aperture radius and λ the wavelength. Since we are launching narrow pulses from extended apertures of large dimensions, one might wonder which radius to use; that of the pulse or the maximum aperture radius. In particular, for a Gaussian beam the waist of the beam is usually taken as the effective R. Such a value is used to determine the Rayleigh diffraction length. The same is true even if the Gaussian beam is generated from a 'static' aperture of a much larger radius. A Gaussian beam of radius 2.83 mm and frequency $f = 19.1$ THz has a Rayleigh limit equal to 1.6 m. This value should be viewed in the light of the decay patterns of the three investigated LW pulses. Figure 4 shows that they have decay rates less than $(1/R)$ up to a few kilometres.

On the other hand, one may argue that the use of the maximum radius of the aperture $R_{\max}$ in the expression for the Rayleigh limit would yield a diffraction length much larger than few kilometres. However, in this case we are exciting a pulse having a transverse extension ~ 7 m. Thus, we claim that LW pulses generated from dynamic apertures are

suitable for applications that require highly focused narrow pulses with large penetration depths. Such applications may include medical radiology, high resolution scanning and secure signalling. A dynamic aperture is an efficient contraption capable of sending narrow pulses several orders of magnitude farther than comparable 'static' radiators. Nevertheless, there remains the delicate problem of how to characterize the diffraction lengths of such dynamic sources.

To resolve this situation Hafizi and Sprangle [8] deduced a diffraction length for apertures that vary their size with time. Their diffraction length depends on the maximum and minimum radii of the generating dynamic aperture or equivalently one has

$$Z_{\mathrm{HS}} = \frac{R\kappa}{\Delta\chi} \tag{6.1a}$$

where $\kappa \equiv \omega_{\max}/c$, $\omega_{\max}$ is the maximum frequency contributing to the spectrum and R is the radius of the aperture (for a dynamic aperture one should take $R = R_{\max}$). One should note that $\Delta\chi$ is approximately the reciprocal of the minimum radius $R_{\min} = \mathrm{O}(4/\chi_{\max})$. Hence, equation (6.1*a*) may be rewritten as

$$Z_{\mathrm{HS}} = \mu R_{\max} R_{\min} \left(\frac{\omega_{\max}}{c}\right). \tag{6.1b}$$

Here μ is a numerical factor of order O(1). It is clear from (6.1*b*) that for a narrow waisted pulse generated by a dynamic aperture, the enhancement in the diffraction length over a 'static' radiator is equal roughly to the ratio $R_{\max}/R_{\min}$. For sources of ultra-wide bandwidths, there is a formal problem of determining the highest frequency components. There have been some attempts to work with an effective frequency that can be derived for any ultra-wide spectrum [6, 16]. However, we would like to point out that in such inclusive definitions of κ, certain features may not be observed. For example, we cannot see that the centroid of the PFWM pulse will hold together for longer distances (~ 80 m) before it starts to decay, or that the centroid of the MFWM will decay at a rate slower than that of PFWM for distances $z > 1$ km. Definitions as that introduced by Hafizi and Sprangle [8] give good estimates of the behaviour of the generated LW fields in a broad sense. This is particularly true for pulses generated by dynamic apertures whose size varies monotonically. In order to see how our three examples agree with the Hafizi–Sprangle diffraction length [8], we need to determine the maximum effective radii of the three apertures considered in the preceding sections. For each case we deal with the initial excitation on the aperture which is given by (4.1). The maximum effective radius of the FWM is directly deduced from (4.6) by setting $t = 4T$ and $z = 0$. Considering only the real part we have the following excitation of the aperture

$$\Psi_i(\rho, t) = \frac{\mathrm{e}^{-t^2/4T^2}}{4\pi\sqrt{a_1^2 + (ct)^2}} \cos(\tan^{-1}(ct/a_1) + \beta ct - \beta\rho^2 ct/(a_1^2 + (ct)^2))\mathrm{e}^{-\beta\rho^2 a_1/(a_1^2+(ct)^2)} \tag{6.2}$$

at $t = 4T$. In figure 12(*a*) we have plotted $|\Psi_i/(\Psi_i)_{\max}|^2$ using (6.2). We show only the maximum values of the *cosine* term which occurs at

$$\rho = [((a_1^2 + (cT)^2)/\beta cT)(\tan^{-1}(cT/a_1) + \beta cT + 2n\pi)]^{1/2} \tag{6.3}$$

where n is an integer whose values are $0, 1, 2, \ldots$, etc. The maximum radius of the aperture is defined as the radius at which the power amplitude of the field on the aperture drops to $(1/\mathrm{e}^2)$ of its maximum value at $t = 4T$. This definition is quite severe because the radius is estimated at the time when the illumination of the aperture is turned off. The field exciting the aperture is already too sparse. At such an instant, the maximum field amplitude is about

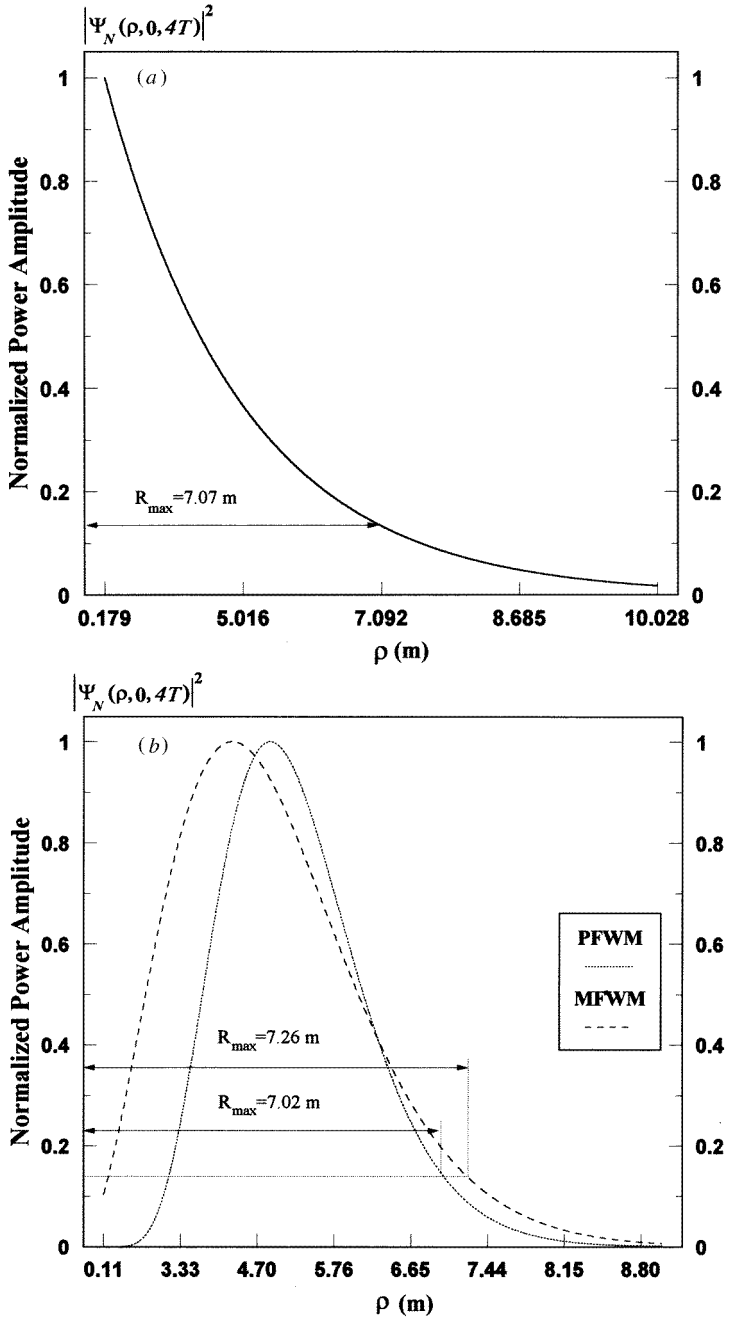

Figure 12. The field distribution of the excitation of the aperture at $t = 4T$.

a_1 times its value at $t = 0$, when we have the most intense illumination of the aperture. From figure 12(a) the maximum effective radius of the FWM is $R_{\max} = 7.07$ m. We notice also from this figure that most of the significant components of the field are located at low values of ρ and the power distribution over the aperture resembles to a great extent that

of the χ-spectrum. For the case of the PFWM the maximum radius is calculated from the real part of (2.6) which is plotted in figure 12(*b*) (cf the dotted curve) at values of ρ that correspond to the maximum of the function. These values of ρ were found to be

$$\begin{aligned}\rho &= [((a_1^2+(cT)^2)/\beta cT)(\tan^{-1}(cT/a_1)-\pi/2+2n\pi)]^{1/2} \qquad 1 \leqslant n \leqslant 476\\ \rho &= [((a_1^2+(cT)^2)/\beta cT)(\tan^{-1}(cT/a_1)+\pi/2+2n\pi)]^{1/2} \qquad n > 476\,.\end{aligned} \tag{6.4}$$

From the figure it is clear that $R_{\max} = 7.02$ m. Similarly the maximum radius of the MFWM is calculated from the real part of (2.8), where for ($ct \gg a_1$) the broken curve in figure 12(*b*) shows the amplitudes of the illumination at ρ values given by

$$\rho = [((a_1^2+(cT)^2)/\beta cT)(\tan^{-1}(cT/a_1)+\beta cT(1+a_2^2/(a_1^2+(cT)^2))+2n\pi)]^{1/2}\,. \tag{6.5}$$

In this case, $R_{\max} = 7.26$ m. Again, the power distribution on the aperture is similar to that of the spatial spectrum shown in figure 1. This demonstrates the relation between the spatial spectrum and the distribution of the field on the aperture.

We would like to point out that we have chosen $cT = 6.25$ mm for the FWM aperture and $cT = 2.5$ mm for both the PFWM and MFWM in order that the maximum extensions of the three sources become equal. It has been shown in the preceding analysis that the three apertures acquire maximum radii ~ 7 m. Because the sizes of the three sources are taken to be equal, a comparison of the decay behaviour (cf figure 4) of their radiated pulses should reflect solely the role of the spectral content of their excitations.

Considering the diffraction length of the three cases, and starting as usual with the FWM, we have $\Delta\chi = 1415$ m^{-1}, $\omega_{\max} = 1.2 \times 10^{14}$ rad s^{-1} and $R_{\max} = 7.07$ m. Substituting in (6.1*a*) we have $Z_{\rm HS} = 1998.8$ m. For the PFWM we have $\Delta\chi = 1927.5$ m^{-1}, $\omega_{\max} = 3.26 \times 10^{14}$ rad s^{-1} and $R_{\max} = 7.02$ m. These values give $Z_{\rm HS} = 3955.2$ m. Finally, for the MFWM, the quantities $\Delta\chi = 2537.5$ m^{-1}, $\omega_{\max} = 3.87 \times 10^{14}$ rad s^{-1} and $R_{\max} = 7.26$ m yield $Z_{\rm HS} = 3688.4$ m. It can be inferred from figure 4 that these estimates of the diffraction length correspond to the distances travelled by the waves before the amplitude of their centroids drop to about $(1/e^4)$ of their values on the aperture. We should mention here that a different definition of the maximum spectral width may change the $Z_{\rm HS}$ value. For example, choosing a $(1/e^2)$ criterion for the spectral width instead of $(1/e^4)$ reduces $Z_{\rm HS}$ calculated by a factor of $\sqrt{2}$. Again we emphasize the fact that certain near-far-field features exhibited by our examples are effaced by an analysis of the type given above. Specifically, the better initial performance of the PFWM followed by an improved decay pattern of the MFWM at larger distances cannot be deduced from an inclusive definition of the diffraction length similar to that calculated above.

7. Conclusion

In this work, we have studied three excitation schemes of dynamic apertures. One of these uses the FWM field and has been investigated in detail in another paper [1]. The other two utilize variations of the FWM excitation, the spectral components of which are distributed in a different manner. Whereas the FWM has most of its significant components located at the lower end of its spectrum, the other two examples have most of their spectral components located at higher frequencies. It has been demonstrated that the shape of the spatial spectrum affects the rate of decay of the pulse. In the near-far-field range, the LW pulses can hold out better than equivalent pulses radiated from static radiators [1]. Such an enhancement has been shown to be roughly of the order of the ratio $R_{\max}/R_{\min}$. Thus for dynamic apertures having equal maximum radii, the radiated LW pulses typified by narrower focused waists should hold out longer before they start to decay. Figure 4 shows that this is true for both

the PFWM and MFWM pulses exhibiting slower decay rates than the FWM pulse in the near-field range. For the FWM pulse $R_{\min}$ is equal to $4/\chi_{\max}$. A slower decay, hence, follows from increasing the spatial bandwidth. Nevertheless, pulses like the PFWM and MFWM can reduce $R_{\min}$ while keeping the anticipated increase in $\chi_{\max}$ at bay.

The shape of the spatial spectrum has a direct effect on the range through which a pulse can travel before it starts decaying, and it also determines the rate of decay of the pulse. For example, the generating field of the PFWM pulse has no low-frequency components. As a result, this pulse holds itself for longer distances before it starts decaying even though it has approximately the same $\omega_{\max}$ as the MFWM. The amplitude of the latter initially starts to fall off at a faster rate; however, it takes over at larger distances. This is the case because its spectrum exhibits extended tails of relatively small strength. Far from the aperture, these spectral components come into play, and the amplitude of the centroid of the MFWM falls off at a slower rate than that of the PFWM. One should also note that the slow-down in the decay rates of the PFWM and the MFWM has been achieved primarily because of the decrease in $R_{\min}$ without increasing the frequency bandwidth as would have been required for the case of the FWM. As such one can regard the latter as having a relatively larger effective bandwidth and thus expect its decay to slow down as we get farther away from the aperture. This effect can be seen in figure 4 where it is clear that the amplitudes of the three pulses are almost equal at $z = 2500$ m, even though the MFWM and PFWM have a much slower decay rate in the near field region.

To further our understanding of the basic factors underlying the amplitude fall off of a LW pulse as it propagates away from its generating aperture, we have carried out a detailed analysis of the depletion of the spectral components with distance. This has been done for a dynamic aperture excited for a finite time controlled by a Gaussian time-window. Such an aperture has an effective radius that shrinks and expands monotonically. It has been shown that as the pulse travels away from the aperture, high oscillations are introduced into the integrand of (5.6). These oscillations appear at the lower end of the spectrum and progressively deplete the higher frequency components as the pulse travels to longer distances from the source. Hence, a clever design of the shape of the spectral ω-windows to reduce the oscillations introduced into them with distance can slow down the decay rate of the associated LW pulse.

The aforementioned effects on the propagation of the LW pulses in the near-far-field region might be overshadowed in inclusive definitions of a diffraction length [6, 16]. Such definitions usually give a diffraction limit that depends on the maximum size of the aperture, the bandwidth of the spatial (or transverse) χ-spectrum and the maximum value of the temporal ω-spectrum. Various authors set different criteria for defining $\Delta\chi$ and $\omega_{\max}$. For example, one can use either a 3 dB point, a half-power width or even adopt a more strict criterion (e.g. the $(1/e^4)$ used in this work) to try to include the effects of the extended tails. This is just a pedagogical issue that does not add anything new to the physics of the problem. The aforementioned definitions of a diffraction length give a good estimate, in a broad sense, of the behaviour of a generated LW as it propagates in the near-far-field region. Our three examples show good agreement with the predicted diffraction lengths, apart from minor differences, such as those observed in the comparison between the PFWM and MFWM pulses. Namely, that the PFWM holds better at smaller distances, and that MFWM takes over at larger ones.

The main issue here is the following: can we use two apertures of the same maximum radii, both having almost the same ω- and χ-spectral widths, with one of the two apertures generating LW pulses that decay at a slower rate than the pulses generated by the other? Along the same vein one may wonder if we should hold to inclusive definitions of diffraction

limits when we discuss the dispersion of ultra-wide-bandwidth pulses, or does it suffice to set up criteria that allow us to use our apertures and source generators in a more efficient way? We claim that the quantitative analysis of the depletion of the spectral components of propagating pulses presented in this work is an effective approach to resolving such issues.

The time dependence of the radius of the investigated aperture reflects its dynamic character. Other suggestions to generate other FWM-like pulses are based on moving sources, the speeds of which are very close to the velocity of light [17–20]. Among such schemes the works of Borisov and Utkin [18, 19] and that of Palmer and Donnelly [20] are prominent. Such moving source schemes are derived from Green's function variables. The translation of the source with time should be contrasted to the expansion of our aperture; they both allude the dynamic nature of the sources needed to generate LW pulses. In fact, one may argue that dynamic apertures represent a *temporal* focusing scheme. This should be contrasted with *spatial* focusing using curved apertures. For dynamic sources, the excitation time sequence of the illumination wavefield can control the focusing depth of the generated LW pulses. Applications requiring fast and frequent changes in the focusing depth can benefit from a *temporal* focusing procedure which may become superior to the mechanically rigid *spatial* one. We believe that a combination of the two schemes can provide more possibilities for existent and new applications.

References

[1] Shaarawi A M, Besieris I M, Ziolkowski R W and Sedky S M 1995 Generation of approximate focus wave mode pulses from wide-band dynamic Gaussian aperture *J. Opt. Soc. Am.* A **12** 1954

[2] Shaarawi A M, Ziolkowski R W and Besieris I M 1995 On the evanescent fields and the causality of the focus wave modes *J. Math. Phys.* **36** 5565

[3] Ziolkowski R W, Besieris I M and Shaarawi A M 1993 Aperture realizations of the exact solutions to homogeneous wave equations *J. Opt. Soc. Am.* A **10** 75

[4] Brittingham J N 1983 Focus wave modes in homogeneous Maxwell's equations: transverse electric mode *J. Appl. Phys.* **54** 1179

[5] Ziolkowski R W 1985 Exact solutions of the wave equation with complex source locations *J. Math. Phys.* **26** 861

[6] Ziolkowski R W 1992 Properties of electromagnetic beams generated by ultra-wide bandwidth pulse-driven arrays *IEEE Trans. Antenna Propagat.* **AP-40** 888

[7] Ziolkowski R W 1991 Localized wave physics and engineering *Phys. Rev.* A **44** 3960

[8] Hafizi B and Sprangle P 1991 Diffraction effects in directed radiation beams *J. Opt. Soc. Am.* A **8** 705

[9] Froberg N, Mack M, Hu B B, Zhang X-C and Auston D H 1991 500 GHz electrically steerable photoconducting antenna array *Appl. Phys. Lett.* **58** 446

[10] Besieris I M, Shaarawi A M and Ziolkowski R W 1989 A bi-directional traveling plane wave representation of exact solutions of the scalar wave equation *J. Math. Phys.* **30** 1254

[11] Durnin J, Miceli J J and Eberly J H 1987 Diffraction-free beams *Phys. Rev. Lett.* **58** 1499

[12] Abramowitz M and Stegun I A 1972 *Handbook of Mathematical Functions* (New York: Dover)

[13] Ziolkowski R W and Lewis D K 1990 Verification of the localized wave transmission effect *J. Appl. Phys.* **68** 6083

[14] Ziolkowski R W, Lewis D K and Cook B D 1989 Experimental verification of the localized wave transmission effect *Phys. Rev. Lett.* **62** 147

[15] Morse P M and Feshbach H 1953 *Methods of Theoretical Physics* (New York: McGraw-Hill) section 11.3

[16] Ziolkowski R W and Judkins J B 1992 Propagation characteristics of ultra-wide bandwidth pulsed Gaussian beams *J. Opt. Soc. Am.* A **9** 2021

[17] Chatzipetros A A 1994 Sources of localized waves *PhD Dissertation* VPI & SU, Blacksburg, Virginia

[18] Borisov V V and Utkin A B 1993 Electromagnetic fields produced by the spike pulse of hard radiation *J. Phys. A: Math. Gen.* **26** 4081

See also La Zarev Y N and Petrov P V 1994 Generation of an intense directed, ultra short electromagnetic pulse *JETP Lett.* **60** 634

[19] Borisov V V and Utkin A B 1994 Some solutions of the wave and Maxwell's equations *J. Math. Phys.* **35** 3624

[20] Palmer M R and Donnelly R 1993 Focused wave modes and the scalar wave equation *J. Math. Phys.* **34** 4007